SCIENCE CHINA
Earth Sciences

• RESEARCH PAPER •

June 2015 Vol.58 No.6: 929–938
doi: 10.1007/s11430-015-5059-9

A method for solving relative dispersion of the cloud droplet spectra

LIU Yu* & LI WeiLiang

Chinese Academy of Meteorological Sciences, Beijing 100081, China

Received September 13, 2014; accepted February 11, 2015; published online April 10, 2015

The relative dispersion of the cloud droplet spectra or the shape parameter is usually assumed to be a constant in the two-parameter cloud microphysical scheme, or is derived through statistical analysis. However, observations have revealed that the use of such methods is not applicable for all actual cases. In this study, formulas were derived based on cloud microphysics and the properties of gamma function to solve the average cloud droplet radius and the cloud droplet spectral shape parameter. The gamma distribution shape parameter, relative dispersion, and cloud droplet spectral distribution can be derived through solving the droplet spectral shape parameter equation using the average droplet radius, volume radius, and their ratio, thereby deriving an analytic solution. We further examined the equation for the droplet spectral shape parameter using the observational droplet spectral data, and results revealed the feasibility of the method. In addition, when the method was applied to the two-parameter cloud microphysical scheme of the Weather Research and Forecast (WRF) model to further examine its feasibility, the modeling results showed that it improved precipitation simulation performance, thereby indicating that it can be utilized in two-parameter cloud microphysical schemes.

cloud droplet spectrum, gamma distribution, relative dispersion, shape parameter, average radius

Citation: Liu Y, Li W L. 2015. A method for solving relative dispersion of the cloud droplet spectra. Science China: Earth Sciences, 58: 929−938, doi: 10.1007/s11430-015-5059-9

Changes in clouds and their optical properties exert a strong influence on the short-wave radiation of the sun and long-wave radiation of the earth-atmosphere system, and alter the balance of the radiation within the earth-atmosphere system. The indirect climate effect from aerosols represents the biggest uncertainty in climate change research (IPCC, 2007), in other words, the effect from clouds is therefore the biggest uncertainty. The complexity of the cloud microphysics parameterization scheme in cloud model and climate model has increased with improvements in computer technology. Two methods are used in cloud microphysical parameterization: one is the bin method through which changes in the cloud droplet distribution can be identified and the optical properties of the clouds can be derived. However, this scheme has limitations in that a large amount of computation is required. The second method is a bulk approach that utilizes the distribution function to depict the cloud droplet distribution, and has been widely used in 3-D cloud model (Xu et al., 1996; Jiang et al. 2000, 2001) and climate model (Lohmann et al., 1999; Curry et al., 2000; Morrison et al., 2008).

The cloud droplet spectral distribution is very important within the bulk approach. Firstly, it affects cloud droplet transformation into rain droplets, namely the cloud liquid automatic conversion rate (Liu et al., 2006b), and hence it influences rainfall and the evolution of clouds. In other words, it influences the aerosol second indirect effect. Secondly, it affects the cloud droplet effective radius, and the cloud droplet effective radius determines the cloud optical

*Corresponding author (email: liuyu@cams.cma.gov.cn)

properties and can therefore influence the aerosol first indirect effect. Liu and Daum (2002) pointed out that the cloud droplet relative dispersion effect exists in the aerosol first indirect effect. The relative dispersion of the cloud droplet spectrum (i.e., the ratio of the standard deviation of the radius to the average radius) can characterize the average deviation of the droplet spectrum to the average radius. When an increase in the aerosol concentration causes the number of cloud droplets to rise, if the cloud water content remains unchanged then the cloud droplet radius will decrease, thereby leading to a subsequent decrease in the cloud droplet effective radius and an increase in the cloud albedo. This is considered as the aerosol first indirect effect. In addition, when the cloud droplet number concentration (CDNC) increases, the cloud droplet spectrum also changes. If the relative dispersion of the cloud droplet spectrum increases with an increase in the CDNC, the reduction in the cloud droplet effective radius becomes less in some extent, namely, the cloud droplet relative dispersion effect will partially offset the first indirect effect; on the contrary, it will enhance the first indirect effect. Observational data show that the cloud droplet relative dispersion either increases (Martin et al., 1994, 2000; Liu et al., 2002; Liu et al., 2006a), or decreases (Ma et al., 2010) with an increase in the CDNC. In addition, observational data have also shown that an increase in the relative dispersion of the droplet spectrum converges along with an increase in the CDNC (Zhao et al., 2006; Lu et al., 2007). This indicates that there is a complex relation between the two, and it is difficult to conclude a general relation. This suggests that there are other factors affecting the cloud droplet relative dispersion.

Apart from using observational data to establish methods for statistical relations, other methods have been used to obtain the cloud droplet spectral distribution, including: (1) establishing a kinetic equation for the cloud droplet spectral shape parameters and deriving a simplified analytic expression for the cloud droplet spectral shape parameters through simplification or presumptions; however, when this method was used in actual cases it failed to deliver desirable results (Khvorostyanov et al., 1999a, 1999b); (2) with simplifications, using the cloud droplet condensation growth equation to derive an analytic expression for the cloud droplet spectral relative dispersion; however, as this method does not take turbulent flow and coagulation into consideration it is only applicable to stratus clouds which have not precipitated (Liu et al., 2006a); (3) establishing a triple-parameter cloud microphysics scheme (Milbrandt et al., 2005b), and increasing the radar reflectivity (six moments) that is used as the predicted variable to derive a shape parameter of the cloud droplet spectral gamma distribution; however, this method cannot offer analytical solutions for the shape parameter and is computation-intensive, hence it has not been widely used in modeling; and (4) developing a cloud microphysics scheme with multiple parameters (Kogan et al., 2012) and establishing a relational expression for the high-order moment of cloud droplets using the bin modeling; this scheme increases the predicted variables and is computation-intensive but offers only limited improvement in results compared with the two-parameter scheme.

Extensive observational data have shown that the gamma function can satisfactorily characterize the cloud droplet spectral distribution (Mason, 1971; Sedunov, 1974; Cotton et al., 1989; Pruppacher et al., 1997). In a variety of bulk approaches, the gamma function with three parameters is used to characterize a cloud droplet distribution, $n(r) = N_0 r^{\mu} \mathrm{e}^{-\lambda r}$, where $n(r)$ is the CDNC in a unit volume of unit radius, and r is the cloud droplet radius; N_0, μ and λ are the parameters, and among them, N_0 is often called intercept, λ is the slope, and μ is related to the spectral width (and is often called the shape parameter) (Ferrier, 1994; Meyers et al., 1997; Cohard et al., 2000; Reisner et al., 1998; Milbrandt et al.，2005a; Morrison et al., 2005). Generally, in the scheme with a single parameter the cloud mass concentration is predicted and is proportional to the cloud droplet spectral three-moment (volume); therefore, parameter λ can be determined, while parameters N_0 and μ remain constant. In a two-parameter scheme, the cloud mass concentration and the total number concentration are forecast, and parameters N_0 and λ can be determined, while parameter μ remains constant.

At present, the triple-parameter scheme offers no analytical solution for parameter μ and is computation-intensive (Milbrandt et al., 2005b). In this paper, we derive a method offering an analytical solution for the cloud droplet triple-parameter gamma distribution by adding an additional formula into the two-parameter scheme through theoretical analysis. It is hoped that by applying this method to the modeling, an improvement can be made to the method currently used in the model based on the statistical relation between the relative dispersion and the CDNC. Our aim was to make preparations for further research on the effect of cloud droplet spectral relative dispersion on the aerosol indirect effect. The proposed method, along with its preliminary test results and application, is described below.

1 Method offering an analytical solution for cloud droplet spectra

The equation of cloud condensational growth (Pruppacher et al., 1997) is

$$\frac{\mathrm{d}m}{\mathrm{d}t} = 4\pi\rho_{\mathrm{w}} r \frac{S}{G}, \tag{1}$$

where m is the droplet mass, r the cloud droplet radius, S supersaturation of the water vapor, ρ_{w} the water density, and

$$G = \left(\frac{L_{\mathrm{v}}}{R_{\mathrm{v}}T} - 1\right)\frac{L_{\mathrm{v}}\rho_{\mathrm{w}}}{K_{\mathrm{d}}T} + \frac{\rho_{\mathrm{w}}R_{\mathrm{v}}T}{D_{\mathrm{v}}e_{\mathrm{s}}}, \tag{2}$$

where T is temperature, D_v the water vapor diffusivity coefficient, K_d the thermal-conductivity coefficient, R_v the gas constant of the water vapor, and e_s the saturated water vapor pressure. For cloud droplets (r >1 μm), the Kelvin and Raoult effects can be ignored. In addition, the ventilation and accommodation effects are ignored.

The integration of eq. (1) for the cloud droplet spectrum leads to

$$\int n(r)\frac{\mathrm{d}m}{\mathrm{d}t}\mathrm{d}r = 4\pi\rho_w \frac{S}{G}\int n(r) r\mathrm{d}r\,. \tag{3}$$

The left side of eq. (3) is the liquid water content change rate due to condensational growth; based on the definition of average radius, eq. (3) is thus changed to

$$\frac{\mathrm{d}L_w}{\mathrm{d}t} = 4\pi\rho_w \frac{S}{G} N r_1, \tag{4}$$

where L_w is the liquid water content, N is the CDNC, and r_1 is the average cloud droplet radius.

Through eq. (4) the average cloud droplet radius r_1 can be derived as:

$$r_1 = \frac{\mathrm{d}L_w}{\mathrm{d}t} \Big/ \left(4\pi\rho_w N \frac{S}{G}\right). \tag{5}$$

In addition, the cloud droplet volume radius is

$$r_3 = \left(\frac{3}{4\pi\rho_w}\right)^{\frac{1}{3}} \left(\frac{L_w}{N}\right)^{\frac{1}{3}}, \tag{6}$$

where r_3 is the cloud droplet volume radius.

In the two-parameter cloud microphysics parameterization, the cloud liquid water content and the CDNC are predicted variables; furthermore, contributions to the liquid water content from the processes such as condensation/vaporization are calculated individually during the liquid water content forecast. Thus, the average cloud droplet radius and the volume radius can be derived through eqs. (5) and (6).

Extensive observations have shown that gamma function is able to effectively characterize the cloud droplet spectra distribution:

$$n(r) = N_0 r^{\mu} \mathrm{e}^{-\lambda r}, \tag{7}$$

where N_0, μ, and λ are all parameters. For the cloud droplet spectra of the gamma distribution, the arbitrary moment of the droplet radius, M_p, is

$$M_p = \left(\frac{1}{\lambda}\right)^p \frac{\Gamma(\mu + p + 1)}{\Gamma(\mu + 1)}, \tag{8}$$

where Γ is the gamma function and p is the order.

By applying eq. (8), the following equation can be obtained:

$$\frac{M_3}{M_1^3} = \frac{r_3^3}{r_1^3} = \frac{(\mu+3)(\mu+2)}{(\mu+1)^2}, \tag{9}$$

and assume that:

$$x = \mu + 1, \tag{10}$$

$$a = \frac{r_3^3}{r_1^3}. \tag{11}$$

Eq. (9) is transformed into:

$$(1-a)x^2 + 3x + 2 = 0, \tag{12}$$

$$x = \frac{-3 \pm \sqrt{9 - 8(1-a)}}{2(1-a)}. \tag{13}$$

As $x = \mu + 1 = \frac{1}{\varepsilon^2}$ (see appendix), where ε is the cloud droplet spectral relative dispersion (ratio of the standard deviation to the average radius), x should be greater than 0. When $a < 1$, there is no solution for x, but when $a > 1$,

$$x = \frac{-3 - \sqrt{9 - 8(1-a)}}{2(1-a)}. \tag{14}$$

Through eq. (14) the shape parameter μ and the relative dispersion ε can be further derived. Parameter λ can subsequently be derived using the average radius or volume radius, and parameter N_0 can be derived using the CDNC.

2 Validation of method

2.1 Comparison between theoretical computational results and observational data

We used the cloud droplet spectral observational data (Ma et al., 2010) from the "Research Project of the Effect of Pollution on Aerosols and Microphysics in Northern China" (IPAC-NC Project, 2005–2008) to test this method. FSSP-100 (Forward Scattering Spectrometer Probe) was used for cloud droplet spectral observations, with a measurement range of 2–47 μm in 15 increments. Aircraft-based observational data from the period 1:50 to 5:30 (UT) on April 16, 2006, were used for analysis, and on that day Moderate Resolution Imaging Spectroradiometer (MODIS) data showed that there was relatively high cloud fraction in North China (90% on average) with a cloud top pressure greater than 700 hPa and a cloud top temperature of approximately 264–273 K (http://gdata1.sci.gsfc.nasa.gov/daac-bin/G3/gui.cgi? instance_id=MODIS_DAILY_L3). Figure 1 shows the cloud droplet spectral distribution at various altitudes (2000–2050, 2050–2100, 2100–2150, 2150–2200, 2200–2250, 2250–2300 and 2300–2350 m, respectively) in North China on April 16, 2006.

Table 1 shows the following information at each altitude: the average cloud droplet radius (r_1), volume radius (r_3), observed relative dispersion (ε) with shape parameter (μ), and relative dispersion (ε_1) with shape parameter (μ_1) calculated based on eq. (14) using the observed average radius (r_1) and volume (r_3). This table shows that the maximum relative deviation of ε and ε_1 is less than 12%, and that the average relative deviation is 6.4%. Figure 2(a) is a correlation scatter diagram of the observed relative dispersion against the calculated relative dispersion. The results show that the calculated relative dispersion is well correlated with the observed data; with a correlation coefficient of 0.978 and a confidence level of 99%. Figure 2(b) is a correlation scatter diagram of the observed shape parameter against the calculated shape parameter, and it can be seen that these two parameters correlate well, as evidenced by a correlation coefficient of 0. 987 and a confidence level of 99%. These results indicate that this method offers a very good solution for deriving the droplet gamma distribution parameter, whether at the cloud top, at the cloud base, or within the cloud.

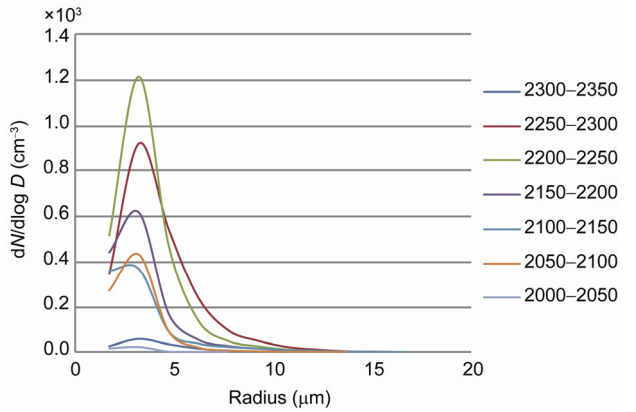

Figure 1 Cloud droplet spectral distribution at various altitudes in North China on April 16, 2006. The altitudes are 2000–2050, 2050–2100, 2100–2150, 2150–2200, 2200–2250, 2250–2300, 2300–2350 m, respectively.

Table 1 Average radius, volume radius, and relative dispersion with shape parameter at various altitudes [a)]

	r_1 (μm)	r_3 (μm)	ε	ε_1	$(\varepsilon_1-\varepsilon)/\varepsilon$ (%)	μ	μ_1
2300-2350 m	3.325	3.381	3.014	2.692	2.580	2.634	2.515
2250-2300 m	4.210	4.162	3.618	3.364	3.397	3.107	2.950
2200-2250 m	0.512	0.479	0.440	0.477	0.527	0.412	0.406
2150-2200 m	0.538	0.498	0.462	0.519	0.589	0.436	0.427
2100-2150 m	4.760	3.843	4.949	8.667	11.761	5.755	5.187
2050-2100 m	2.815	3.358	4.165	3.395	2.601	4.891	5.067
2000-2050 m	2.455	3.032	3.685	2.712	1.883	4.260	4.485

a) r_1 is the average radius, r_3 is the volume radius, ε is the observed relative dispersion, ε_1 is the calculated relative dispersion, μ is the observed shape parameter, and μ_1 is the calculated shape parameter.

2.2 Examples of actual application

We applied the method for solving the cloud droplet relative dispersion to the Weather Research and Forecast (WRF) model, in order to further examine the feasibility of applying this method to the two-parameter cloud microphysics scheme. Because daily rainfall data were available, we hoped that the feasibility study of this method could be carried out based on a comparison of the simulated rainfall data against observed data. The WRF model is a new-generation mesoscale forecast and assimilation system developed by scientists from various research institutes and universities in the USA. To facilitate the application in climate modeling in the future, we chose to apply our method to the Morrison two-parameter cloud microphysics scheme in the WRF3.2 model, as this cloud microphysics scheme is also used in the Community Atmospheric Model version 5 (CAM5). The Morrison two-parameter cloud microphysics scheme includes five hydrometeors: cloud droplets, cloud ice, rain, snow, and graupel. The gamma distribution was used to represent their distributions, as characterized by eq. (7). Since each type was assumed to be spherical, relationship of a mass to radius conforms to the power function. The parameters N_0 and λ of the gamma distribution for each

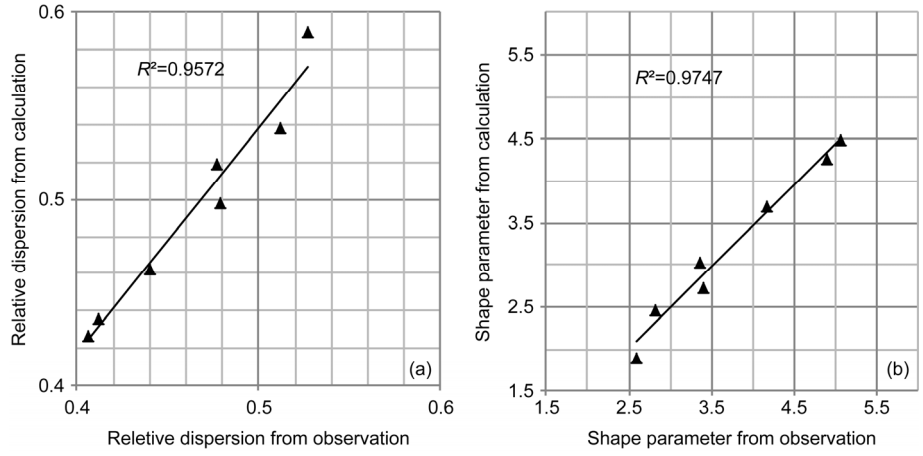

Figure 2 A correlation of the observed and calculated relative dispersion (a) and of the observed and calculated shape parameters (b).

type could then be derived based on the number concentration forecast and the mixing ratio. The parameter μ was predefined, and for precipitation (including rain, snow, and graupel) and cloud ice, the shape parameter was assumed to be 0, μ=0. Thus the distribution of these four could be given by an exponential function, i.e., a Marshall-Palmer distribution. The shape parameter μ for cloud droplets was a function of the CDNC forecast, and the statistics by Martin et al. (1994) were used (Morrison et al., 2009). As our method is applicable for cloud droplets, we only used this method in the determination of the cloud droplet shape parameter μ. Furthermore, to reflect the effect of the cloud droplet spectra on rainfall more accurately, and to facilitate a comparison with the rainfall observed, we revised the computation scheme for the cloud liquid automatic conversion rate, and used the scheme for the cloud liquid automatic conversion rate that takes the cloud droplet spectral distribution into account (Xie et al., 2013):

$$P = P_0 T_C, \tag{15}$$

$$P_0 = 1.1\times10^{10}\left[\frac{\left(1+3\varepsilon^2\right)\left(1+4\varepsilon^2\right)\left(1+5\varepsilon^2\right)}{\left(1+\varepsilon^2\right)\left(1+2\varepsilon^2\right)}\right]N^{-1}L_w^3, \tag{16}$$

$$T_c = \frac{1}{2}\left(x_c^2+2x_c+2\right)\left(1+x_c\right)e^{-2x_c}, \tag{17}$$

$$x_c = 9.7\times10^{-17}N^{3/2}L_w^{-2}, \tag{18}$$

where P is the cloud liquid automatic conversion rate, P_0 is the rate function, T_c is the threshold function, L_w is the liquid water content, and N is the CDNC.

Changes in the liquid water content caused by condensation and vaporization processes can be derived by adjusting the supersaturation, and the formulas used to expedite this are (Straka, 2009):

$$\frac{dL_w}{dt} = \frac{Q_v - Q_{SL}}{\Delta t\left(1+\dfrac{L_v^2 Q_{SL}}{C_p R_v T^2}\right)}, \tag{19}$$

$$\frac{dT}{dt} = \frac{L_v}{C_p}\frac{dL_w}{dt}, \tag{20}$$

where Q_v is the water vapor mixing ratio and Q_{SL} the saturated water vapor mixing ratio. The changing rate of liquid water content by condensation can be obtained through iteration using eqs. (19) and (20). However, as a deviation could possibly occur during adjustment of supersaturation when the CDNC is low, we also made a correction using the correction method by Kogan and Martin (1994). The average cloud droplet radius was then derived using eq. (5), and the relative dispersion and shape parameter were subsequently calculated using eq. (14).

Continuous rainfall occurred in East China from March 25 to March 26, 2013 and Figure 3(a) shows the total amount of precipitation measured within 24 h from 08:00 on March 25 to 08:00 on March 26, 2013 (Beijing time). The figure shows large areas of precipitation in the area of Central China, the northern part of South China, and the eastern part of Southwest China. Regions with heavy rainfall had a belt-shaped distribution, stretching from northern Guangxi to western Fujian via southern Hunan and central Jiangxi. The rainfall reached its peak at the border between Guangxi, Hunan, and Guizhou (with a maximum value exceeding 80 mm); there was a secondary rainfall center in central Jiangxi (with precipitation exceeding 40 mm), and a further precipitation center in northern Hubei (with precipitation exceeding 30 mm). MODIS satellite data show that the cloud top temperature in the region (23°N–29°N, 105°E–110°E) during the day exceeded 273.0 K, implying that the cloud cover in this region during the day was warm cloud. Cloud top temperatures in the other precipitation areas were below 273.0 K.

In order to test our scheme, we simulated the precipitation in China from 08:00 on March 25 to 8:00 on March 26, 2013 (Beijing time), and performed three simulation experiments as follows: (1) using the original scheme for the cloud liquid automatic conversion rate, called as experiment A; (2) using eq.s (15)–(18) for the cloud liquid automatic conversion rate, called as experiment B; and (3) solving the shape parameter and adding it to the scheme of experiment B, called as experiment C. The horizontal resolution of the model was 27 km and there were 40 vertical levels.

Figure 3(b) shows the precipitation results in experiment A. As displayed in the figure, the precipitation distributions from the modeling were close to the measurement data, and the heavy precipitation area was also belt-shaped. However, compared with the measurement data, there was a deviation in terms of the central position of the heavy precipitation area, with the center of the heaviest rainfall area being in the north-east area in Guangxi. In addition, the maximum precipitation exceeded 100 mm, which was greater than that of the measurement data. There were two secondary heaviest precipitation centers, one at the border between Guangxi and Hunan, and the other in southern Hunan, and the central precipitation magnitude was higher than 80 mm, but the ranges of these two secondary centers were relatively small. Figure 3(c) shows the precipitation results from experiment B, and Figure 3(e) shows the difference between the results from experiment B and those of experiment A. It can be seen in Figure 3(c) and (b) that the results from experiment B and A were close, as evidenced by the similar precipitation distribution and the rainfall. Figure 3(e) also supports that the differences between the two experiments were slight, as evidenced by a precipitation difference of less than 5 mm on average for most areas, but the difference was relatively greater in the heavy-precipitation zone in Hunan (higher than 5 mm), and the secondary heaviest zone in Hunan was slightly larger than the observed data. Overall,

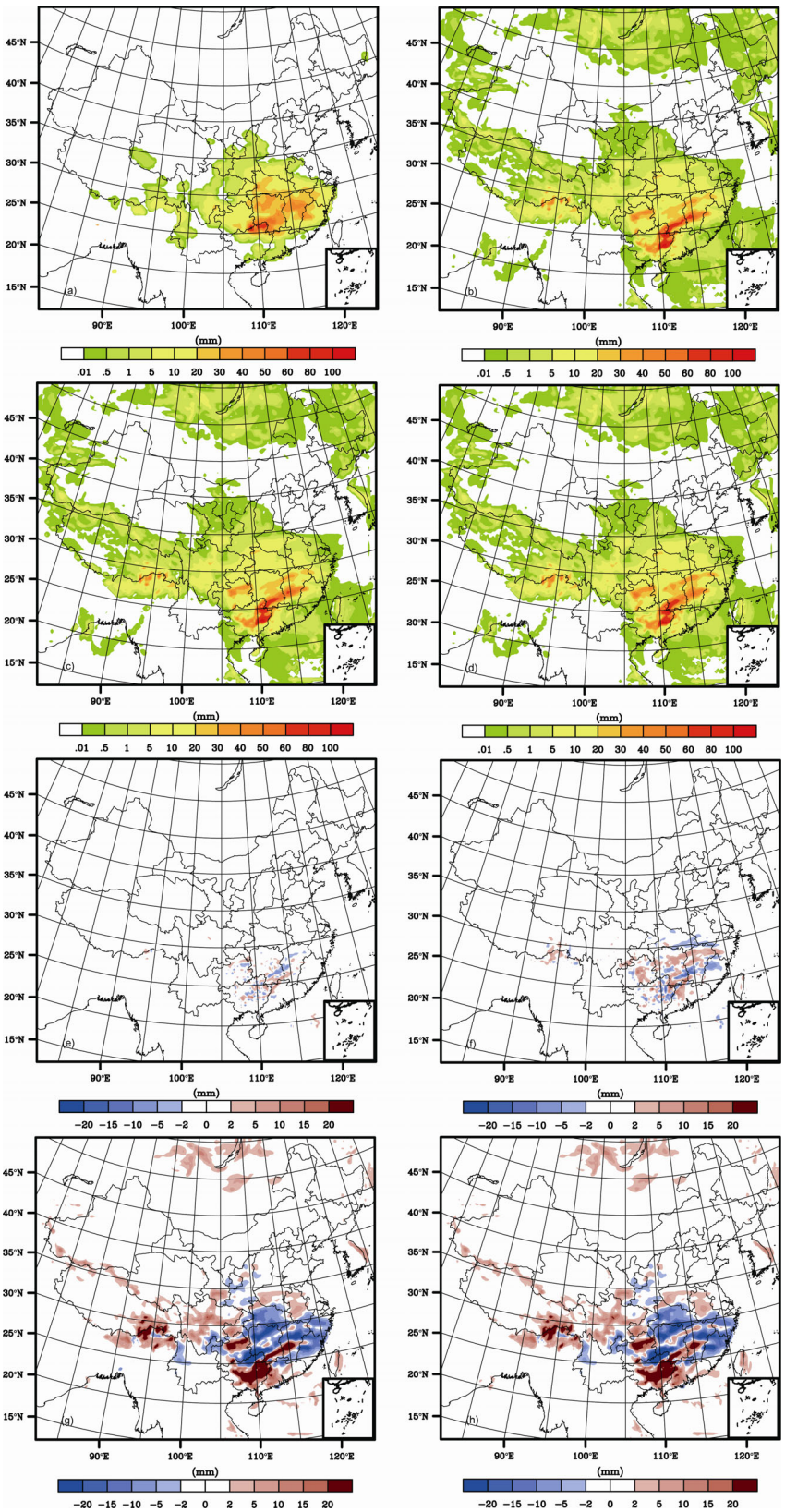

Figure 3 Precipitation from 08:00 on March 25 to 08:00 (Beijing time) on March 26, 2013. (a) observed precipitation; (b) results from the Morrison scheme (experiment A); (c) results from the revised Morrison scheme (experiment B); (d) results from the revised Morrison scheme with the addition of solving the cloud droplet spectra (experiment C); (e) results after subtracting experiment A results from experiment B results; (f) results after subtracting experiment B results from experiment C results; (g) results after subtracting observed data from experiment B results; (h) results after subtracting observed data from experiment C results.

the differences between experiment A and B were not significant.

Figure 3(d) shows the precipitation results derived from experiment C, and Figure 3(f) shows the differences of precipitation between experiment C and B. It can be seen in Figure 3(d) and 3(c) that the results from experiment C and B were close. However, despite the close proximity of the results, the difference was greater than that between experiment B and A. Figure 3(f) shows that the precipitation increased at the border between Guangxi and Hunan, decreased in northeastern Guangxi, and decreased in the heavy-precipitation zone in the Hunan region and western Jiangxi. These changes led to a reduction of the rainfall in northeastern Guangxi (where there was a reduction in the size of the areas receiving amounts higher than 100 mm), and led to an increase in the amount of precipitation at the secondary center of heaviest precipitation (at the border between Guangxi and Hunan), where there was an expansion of the area receiving more than 80 mm of precipitation. In addition, the secondary center of the area with heaviest precipitation (in Hunan) vanished, resulting in a third-heaviest precipitation center located in the heavy precipitation area of Jiangxi, with a rainfall of over 50 mm, and giving the largest precipitation difference which exceeded 10 mm (approximately 15% more than the observed rainfall). The secondary center of the precipitation region at the border between Guangxi and Hunan was closer to the center of the strong precipitation region observed from the measurement data, and the precipitation center in the Jiangxi region was also more consistent with the center of the secondary heaviest precipitation region observed from the actual data. These results indicate that experiment C derived a precipitation distribution closer to the measurement, but it achieved only a limited improvement in terms of the center of the heavy precipitation area in northeastern Guangxi, i.e., this large deviation failed to be significantly improved. Figure 3(g) shows the differences between the precipitation results in experiment B and those of the observed data, and Figure 3(h) shows the differences between the precipitation results in experiment C and the observed data. a comparison of Figure 3(g) and 3(h) shows that the experimental results from experiments C and B were similar. As shown in Figure 3(h), the dark red areas in southern Hunan and southern Jiangxi decreased (the difference exceeded 20 mm), the blue areas in the north-central region in Hunan, north-central region in Jiangxi and southern Hubei decreased (the difference exceeded 15 mm), and the changes in the other areas were insignificant. The changes demonstrated in Figure 3(h) clearly indicate that experiment C significantly improved the prediction performance, yielding the results closer to those of the observed data.

Figure 4(a) shows the total 24-hour rainfall between 08:00 on March 23 and 08:00 on March 24, 2013 (Beijing time). As shown in the figure, there were large precipitation areas in Central China, most regions of South China, and south-east of East China. The heavy precipitation areas showed a belt-shaped distribution, extending from northern Guangxi to northwestern Fujian, via southern Hunan and north-central Jiangxi. The border region between Fujian, Jiangxi, and Zhejiang received the highest rainfall (with a maximum value exceeding 40 mm), followed by the border of Guangxi and Hunan (with a maximum value exceeding 20 mm). In addition, the following areas received snowfall: Liaoning, a major part of Jilin in Northeast China, and a part of Inner Mongolia (with a maximum snowfall exceeding 10 mm). One area of snowfall occurred in each of northwestern Xinjiang and northern Tibet. MODIS satellite data shows that the regional (20°N–27°N, 105°E–117°E) cloud top temperature during daytime was higher than 273.0 K, and therefore the clouds were warm cloud. The cloud top temperatures in other precipitation areas were lower than 273.0 K, but temperatures in most regions south of latitude 25ºN throughout the whole day were higher than 273.0 K.

We carried out two simulations for precipitation in China during the period 08:00 on March 23 to 08:00 on March 24, 2013 (Beijing time): (1) eq.s (15)–(18) were used to calculate the cloud liquid automatic conversion rate (called experiment B1); and (2) the solving of the shape parameter was added into the scheme based on experiment B1 (called experiment C1). Figure 4(b) shows the precipitation results from experiment B1. It can be seen from the figure that the simulated precipitation distribution was close to the observed data, indicating that the precipitation distribution can be simulated by this model for the aforementioned four regions, in particular for southeastern and northeastern China. The model reproduced the precipitation distribution over southeastern China well. The modeled distribution of heavy precipitation areas was also belt-shaped; however, compared with the observed data the position of the heavy precipitation area in Jiangxi deviated, and the precipitation intensity was higher than the observed data, especially in the areas of Guangxi, Hunan, and Jiangxi. Figure 4(c) shows the differences in the precipitation between experiment C1 and B1. As displayed in the figure, the differences between the two experiments were more evident for the rainfall data in the southeastern region, but no significant difference was observed in snowfall in the northeastern region, Xinjiang, and Tibet areas. The reason for this is that our method only affects the calculation of cloud droplets. For southeastern China, experiment C1 derived a higher simulated rainfall in northeastern Fujian (particularly in the offshore area) and improved the simulation when compared with experiment B1. For the heavy precipitation areas in Guangxi, Hunan, and Jiangxi, experiment C1 derived a lower-simulated rainfall, leading to an improvement of the estimates from experiment B1 in which the rainfall was too high. The extent of these changes was mostly within 10 mm, and the characteristics of the precipitation distributions remained unchanged, indicating that the improvement on precipitation simulation by experiment C1 was limited.

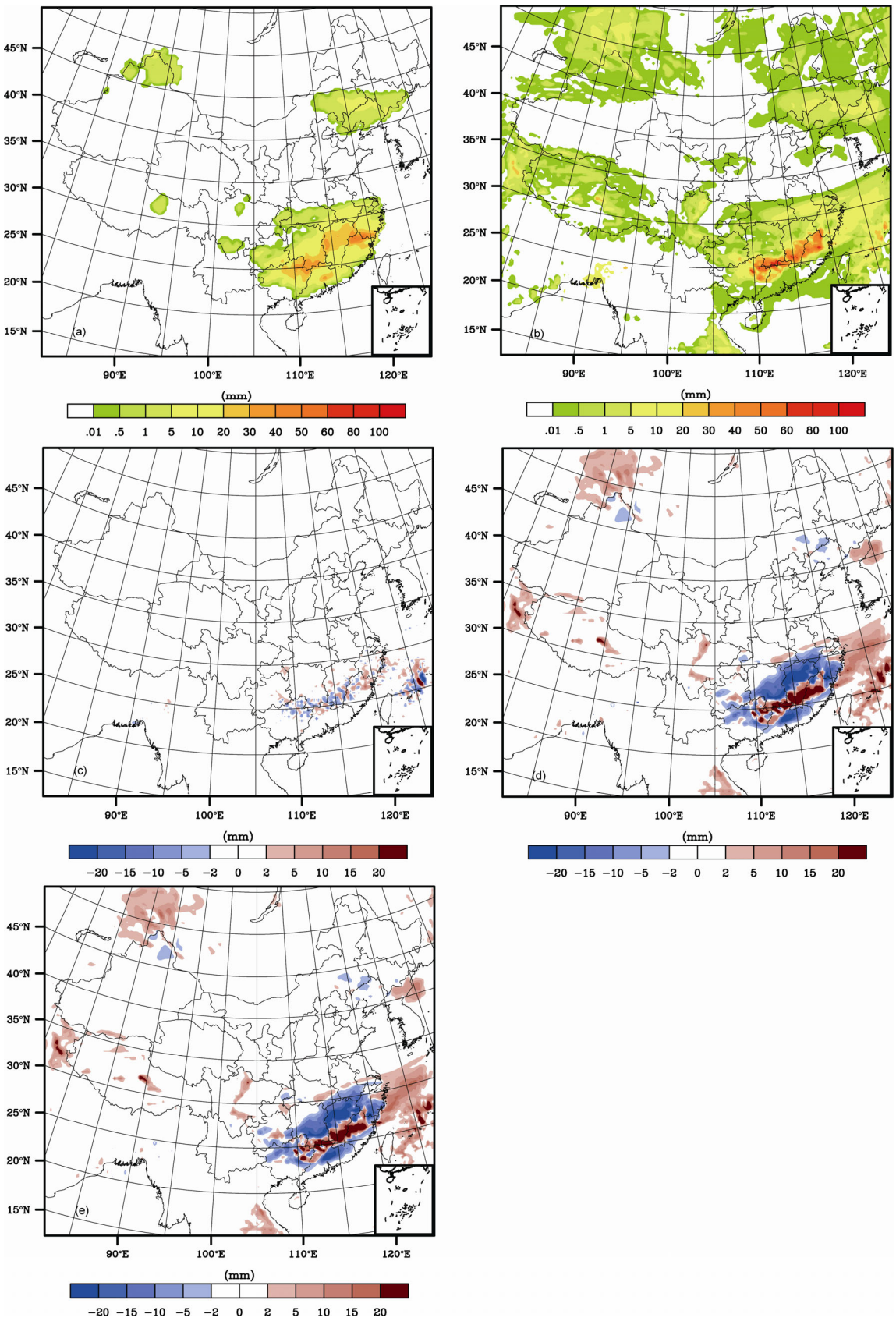

Figure 4 Precipitation falling between 08:00 on March 23 and 08:00 on March 24, 2013. (a) observed precipitation quantity; (b) results from the revised Morrison scheme (experiment B1); (c) results after subtracting results of experiment B1 from those of C1; (d) results after subtracting observed data from experiment B1 results; (e) results after subtracting observed data from experiment C1 results.

Figure 4(d) shows the differences between the results of precipitation derived from experiment B1 and that of the observed data, and Figure 4(e) shows the differences between the results of precipitation from experiment C1 and the observed data. A comparison of Figure 4(d) and 4(e) shows that the results from experiment C1 and B1 are similar. Figure 4(e) demonstrates a decrease in the dark red areas where the differences exceeded 20 mm, and an expansion of white areas in southern Hunan and at the borderline between northeastern and northwestern Guangxi. In addition, in southern Hunan and at the borderline between southern Jiangxi and northern Guangdong, there was a decrease in the dark red areas with a difference exceeding 20 mm, resulting in a discontinuous distribution of the dark red areas, but in the other regions the dark red areas only decreased slightly, showing an insignificant difference. These results indicate that experiment C1 improved the simulation and derived results that were more consistent with the observed data.

A comparison of the two simulations shows that our method was able to improve the precipitation simulation to a certain extent, and this capability was manifested mainly in a simulation of rainfall intensity. As our method was aimed mainly at cloud droplets, it did not significantly improve snowfall the simulation, but the improvement in rainfall simulation suggests that our method is feasible and can be used in a two-parameter cloud microphysics scheme.

3 Summary

Through theoretical derivation, we developed a solution to solve the average cloud droplet radius (eq. (5)) and derived an equation (eq. (14)) to solve the cloud droplet spectral shape parameter. The shape parameter for cloud droplet spectral gamma distribution, or relative dispersion, can be obtained through eqs. (5), (6), and (14). In other words, the shape parameter for cloud droplet spectral gamma distribution, relative dispersion, and cloud droplet spectral distribution can be derived using the average cloud droplet radius, volume radius, and their ratio. Theoretically, the triple-parameter cloud droplet spectral distribution can be solved using the equations for average cloud droplet radius, mass concentration (volume radius), and CDNC, e.g., the triple-parameter gamma distribution. The advantage of this method is that it leads to an analytical solution, which can be conveniently applied to different models.

To verify our method, we performed a comparison of observed cloud droplet spectral data and computed the results using eq. (14). These computed results were very consistent with the observed data, thus proving the feasibility of the proposed method. Our method was then applied to a two-parameter cloud microphysics scheme in the WRF model to solve the shape parameter. The rainfall results of simulation experiments for March 23, 2013 and March 25, 2013 indicated that our method was able to improve the rainfall simulation to a limited extent.

In summary, therefore, this method is feasible and can be applied to two-parameter cloud microphysics schemes. This study provided a theoretical methodology for further exploration of the cloud droplet relative dispersion effect within the aerosol indirect effect.

This work was supported by National Basic Research Program of China (Grant No. 2011CB403406). We give special thanks to Prof. Ma Jianzhong from the Chinese Academy of Meteorological Sciences for the observational data used in this work. In addition, we thank the NCAR for the WRF model.

Appendix Correlation between the shape parameter and the relative dispersion

The relative dispersion (ε) is defined as the ratio of the cloud droplet spectral standard deviation to the average radius, i.e.,

$$\varepsilon = \frac{\left[\int n(r)(r-r_1)^2\,\mathrm{d}r \Big/ \int n(r)\,\mathrm{d}r\right]^{1/2}}{r_1}. \tag{A1}$$

Eq. (A1) is then squared, and the right side of the eq. (1) is expanded:

$$\varepsilon^2 = \frac{\int n(r)r^2\mathrm{d}r / \int n(r)\mathrm{d}r - 2r_1\int n(r)r\mathrm{d}r / \int n(r)\mathrm{d}r + r_1^2\int n(r)\mathrm{d}r / \int n(r)\mathrm{d}r}{r_1^2}. \tag{A2}$$

According to the definition of average radius and average squared radius, eq. (A2) is altered to:

$$\varepsilon^2 = \frac{r_2^2 - 2r_1r_1 + r_1^2}{r_1^2}, \tag{A3}$$

$$\varepsilon^2 = \frac{r_2^2}{r_1^2} - 1. \tag{A4}$$

For a gamma distribution based on the formula of arbitrary order moments for radius (eq. (8)), eq. (A4) is altered to:

$$\varepsilon^2 = \frac{\left(\frac{1}{\lambda}\right)^2(\mu+2)(\mu+1)}{\left(\frac{1}{\lambda}\right)^2(\mu+1)^2} - 1, \tag{A5}$$

$$\varepsilon^2 = \frac{(\mu+2)}{(\mu+1)} - 1, \tag{A6}$$

$$\varepsilon^2 = \frac{1}{(\mu+1)}. \tag{A7}$$

Cohard J M, Pinty J P. 2000. A comprehensive two-moment warm microphysical bulk scheme. I: Description and tests. Q J R Meteorol Soc, 126: 1815–1842
Cotton W R, Anthes R A. 1989. Storm and Cloud Dynamics. London: Academic Press. 883
Curry J A, Hobbs P V, King M D, et al. 2000. FIRE arctic clouds experiment. Bull Amer Meteorol Soc, 81: 5–29
Ferrier B S. 1994. A double-moment multiple-phase four-class bulk ice scheme. Part I: Description. J Atmos Sci, 51: 249–280
IPCC. 2007. Climate Change 2007: The Physical Science Basis. Contribution of Working Group I to the Fourth Assessment Report of the Intergovernmental Panel on Climate Change. In: Solomon S, Qin D, Manning M, et al, eds. New York: Cambridge University Press.
Jiang H L, Cotton W R, Pinto J O, et al. 2000. Cloud resolving simulations of mixed-phase arctic stratus observed during BASE: Sensitivity to concentration of ice crystals and large-scale heat and moisture advection. J Atmos Sci, 57: 2105–2117
Jiang H L, Feingold G, Cotton W R, et al. 2001. Large-eddy simulation of entrainment of cloud condensation nuclei into the arctic boundary layer: May 18, 1998 FIRE/SHEBA case study. J Geophys Res, 106: 15113–15122
Khairoutdinov M F, Kogan Y L. 2000. A new cloud physics parameterization for large-eddy simulation models of marine stratocumulus. Mon Weather Rev, 128: 229–243
Khvorostyanov V I, Curry J A. 1999a. Towards the theory of stochastic condensation in clouds. Part I: A general kinetic equation. J Atmos Sci, 56: 3985–3996
Khvorostyanov V I, Curry J A. 1999b. Towards the theory of stochastic condensation in clouds. Part II: Analytical solutions of the gamma distribution type. J Atmos Sci, 56: 3997–4013
Kogan Y L, Martin W J. 1994. Parameterization of bulk condensation in numerical cloud modeles. J Atmos Sci, 51: 1728-1739
Kogan Y L, Belochitski A, 2012. Parameterization of cloud microphysics based on full integral moments. J Atmos Sci, 69: 2229–2242
Liu Y G, Daum P H. 2002. Indirect warming effect from dispersion forcing. Nature, 419: 580–581
Liu Y G, Daum P H, McGraw R, et al. 2006a. Parameterization of the autoconversion process. Part II: Generalization of Sundqvist-type parameterizations. J Atmos Sci, 63: 1103–1109
Liu Y G, Daum P H, McGraw R, et al. 2006b. Generalized threshold function accounting for effect of relative dispersion on threshold behavior of autoconversion process. Geophys Res Lett, 33: L11804, doi: 10.1029/2005GL025500
Lohmann U, McFarlane N, Levkov L, et al. 1999. Comparing different cloud schemes of a single column model by using mesoscale forcing and nudging technique. J Clim, 12: 438–461
Lu M L, Conant W C, Jonsson H H, et al. 2007. The marine stratus/stratocumulus experiment (MASE): Aerosol-cloud relationship in marine stratocumulus. J Geophys Res, 112: D10209, doi: 10.1029/2006JD07985
Ma J Z, Chen Y, Wang W, et al. 2010. Strong air pollution causes widespread haze-cloud over China. J Geophys Res, 115: D18204, doi: 10.1029/2009JD013065
Martin G M, Johnson D W, Spice A, 1994. The measurement and parameterization of effective radius of droplets in the warm stratocumulus clouds. J Atmos Sci, 51: 1823–1842
Mason B J. 1971. Physics of Clouds. Oxford: Clarendon Press. 481
Meyers M P, Walko R L, Harrington J Y, et al. 1997. New RAMS cloud microphysics parameterization. Part II: The two-moment scheme. Atmos Res, 45: 3–39
Milbrandt J A, Yau M K. 2005a. A multimoment bulk microphysics parameterization. Part I: Analysis of the role of the spectral shape parameter. J Atmos Sci, 62: 3051–3064
Milbrandt J A, Yau M K. 2005b. A multimoment bulk microphysics parameterization. Part II: A proposed three-moment closure and scheme description. J Atmos Sci, 62: 3065–3081
Morrison H, Curry J A, Khvorostyanov V I. 2005. A new double-moment microphysics parameterization for application in cloud and climate models Part I: Description. J Atmos Sci, 62: 1665–1677
Morrison H, Thompson G, Tatarskii V. 2009. Impact of cloud microphysics on the development of trailing stratiform precipitation in a simulated squall line: Comparison of one- and two-moment schemes. Mon Weather Rev, 137: 991–1007
Pruppacher H R, Klett J D. 1997. Microphysics of Clouds and Precipitation. Heidelberg: Springer. 954
Pontikis C, Hicks E. 1992. Contribution to the cloud droplet effective radius parameterization. Geophys Res Lett, 19: 2227–2230, doi: 10.1029/92GL02283
Reisner J, Rasmussen R M, Bruintjes T. 1998. Explicit forecasting of supercooled liquid water in winter storms using the MM5 mesoscale model. Q J R Meteorol Soc, 124: 1071–1107
Sedunov Y S. 1974. Physics of Drop Formation in the Atmosphere. New York: Wiley. 234
Straka J M. 2009. Cloud and Precipitation Microphysics. New York: Cambridge University Press. 392
Twomey S. 1977. The influence of pollution on the shortwave albedo of clouds. J Atmos Sci, 34: 1149– 1152
Xie X N, Liu X D, Peng Y R, et al. 2013. Numerical simulation of clouds and precipitation depending on different relationships between aerosol and cloud droplet spectral dispersion. Tellus Ser B-Chem Phys Meteorol, 65: 19054
Xu K M, Randall D A. 1996. Explicit simulation of cumulus ensembles with the GATE Phase III data: Comparison with observations. J Atmos Sci, 53: 3710–3736
Zhao C S, Tie X X, Brasseur G, et al. 2006. Aircraft measurements of cloud droplet spectral dispersion and implications for indirect aerosol radiative forcing. Geophys Res Lett, 33: L16809, doi: 10.1029/2006GL026653